Electrochemically Induced Sol–Gel Deposition of Zirconia Thin Films

Ronen Shacham, Daniel Mandler,* and David Avnir*[a]

Abstract: A novel electrochemical method for deposition of ZrO_2 thin films is described. The films, 50–600 nm thick, were obtained by applying moderate positive or negative potentials (+2.5 V to −1.5 V versus SHE) on conducting surfaces immersed in a 2-propanol solution of zirconium tetra-*n*-propoxide [$Zr(OPr)_4$] in the presence of minute quantities of water (water/monomer molar ratios in the range of 10^{-5} to 10^{-1}), which was the limiting reagent. Oxidative electrochemical formation of solvated H^+ and reductive formation of OH^- catalyze the hydrolysis and condensation of the metal alkoxide precursor. The magnitude of the applied potential and its duration provide a convenient way of controlling the film thickness. The films consist of an amorphous phase, as revealed by XRD measurements. The effects of different parameters, such as the applied potential and its duration, the amount of added water and the current–time characteristics, were studied. A mechanism for the electrodeposition of the zirconia films which is in accordance with our findings is proposed.

Keywords: electrochemistry · sol–gel processes · thin films · zirconia

Introduction

Thin-film deposition of metal oxides and hydroxides by electrochemical methods is a rapidly developing field.[1–16] In a review on this area, Cryston and Lee[2] suggested that electrochemical methods offer simple and inexpensive alternatives to currently used techniques. These methods of deposition can be categorized into three main groups: electrophoretic deposition,[17–24] deposition on electrochemical formation of less soluble metallic species and deposition by electrochemically altering the pH of the solution near the electrode surface.[1–8,10–16] Recently, we employed the last-named approach[25] in a novel electrochemical sol–gel process in which thin films of methylated silica are deposited on conducting surfaces by application of moderate potentials (in the range of −0.5 V to −1.5 V versus Ag/AgCl). We suggested that the variation of the pH near a conductive surface in the presence of the (hydrolyzed) alkoxysilane effected its polymerization. While electrochemical induction of pH changes is known in the context of the formation of insoluble oxides and hydroxides and their subsequent precipitation,[1,3,4,6,7,10,11,13–16] its use for locally effecting the polymerization of sol–gel monomers and increasing their rate of polymerization is, to the best of our knowledge, unknown. Here we extend our methodology[25] to the important family of zirconia coatings, and report on the electrochemically induced formation of these films and convenient thickness control in the range of several hundreds of nanometers.

As ZrO_2 films have already been prepared electrochemically,[4,13–16,26] we highlight the special features of the electrochemical sol–gel approach reported here. First, whereas precipitation of ZrO_2 has been effected by electrogeneration of a base at negative potentials, the electrochemical sol–gel method makes it possible to use both positive potentials (leading to acid-catalyzed polymerization) and negative potentials (leading to base-catalyzed polymerization). Second, the precursor is [$Zr(OPr)_4$] instead of the commonly used Zr salts.[4,13–15] Third, water is used as a limiting reagent in alcoholic medium (in contrast to the standard use of water as both solvent and reagent[4,13–15]). Fourth, a polycondensation process rather than precipitation[4,7,10,13–15] leads to film formation. Fifth, the films are exceptionally smooth,[27] down to a roughness of 0.7 nm for a 5×5 μm area. The convenient control of film thickness by changing the applied potential or the time for which it is applied is a key feature of this method.

[a] R. Shacham, Prof. D. Mandler, Prof. D. Avnir
Institute of Chemistry
The Hebrew University of Jerusalem
Jerusalem 91904 (Israel)
Fax: (+972) 2-658-5319
E-mail: mandler@vms.huji.ac.il
david@chem.ch.huji.ac.il

Results and Discussion

Zirconia-based thin films were electrodeposited from a solution of zirconium tetra-*n*-propoxide [$Zr(OPr)_4$] in 0.1 M $LiClO_4$ in 2-propanol, to which small and controlled amounts of water were added (solution A). Deposition was

© 2004 Wiley-VCH Verlag GmbH & Co. KGaA, Weinheim
DOI: 10.1002/chem.200305469

carried out by applying constant potentials at electrodes while stirring solution A.

Film characterization: The composition of deposited films was determined by elemental analysis (EPXMA, electron-probe X-ray microanalysis) and XRD. In the EPXMA measurements the atomic concentration of zirconium increased with decreasing electron-beam intensity. Since the penetration of the electron beam (ca. 1 μm) exceeded that of the film thickness at high beam intensities, it is evident that as the intensity decreased the fraction of the elements in the film increased. This implies that Zr is the major component of the deposited layer. As expected, XRD (data not shown) revealed that the films are composed of amorphous ZrO_2, due to the low temperature at which deposition took place. This is in complete agreement with previous reports, for example, by Chaim et al.,[15] who deposited ZrO_2 under galvanostatic conditions in aqueous solutions starting from ZrO^{2+} as the precursor. They also observed a very broad XRD peak around $2\theta \approx 30°$. Only annealing at temperatures above 900 K produced a mixture of tetragonal and monoclinic polymorphs of zirconia.[15]

Our as-deposited dried films were exceptionally smooth, as was evident by AFM. Figure 1 shows four samples that were scanned under identical conditions. Whereas bare ITO (Figure 1a) is characterized by lumps that are about 440 nm long (i.e., in the *xy* plane) with an average height of about 34 nm (along the *z* axis), the coated ITO samples are much smoother: The roughness factor (RMS value) of 5×5 μm samples that were coated at negative potential (Figure 1c, d) is about 0.5 nm, and they are smoother than a zirconia film obtained by dip coating (Figure 1b).[4,13–15,17,19,21,23,27,28] To the best of our knowledge, such smooth films have never been reported previously. This suggests that the electrochemical deposition has a significant levelling effect on the surface. Moreover, as the absolute value of the applied potential and its duration increase, the samples become smoother (Figure 1c, d). These observations suggest a deposition mechanism which involves very small clusters that fill the rough contours of ITO. Although stirring was essential to achieve smooth surfaces, the rate of stirring had little effect on the smoothness. The SEM images (not shown) also show highly smooth surfaces over large areas (up to ca. 100×100 μm).

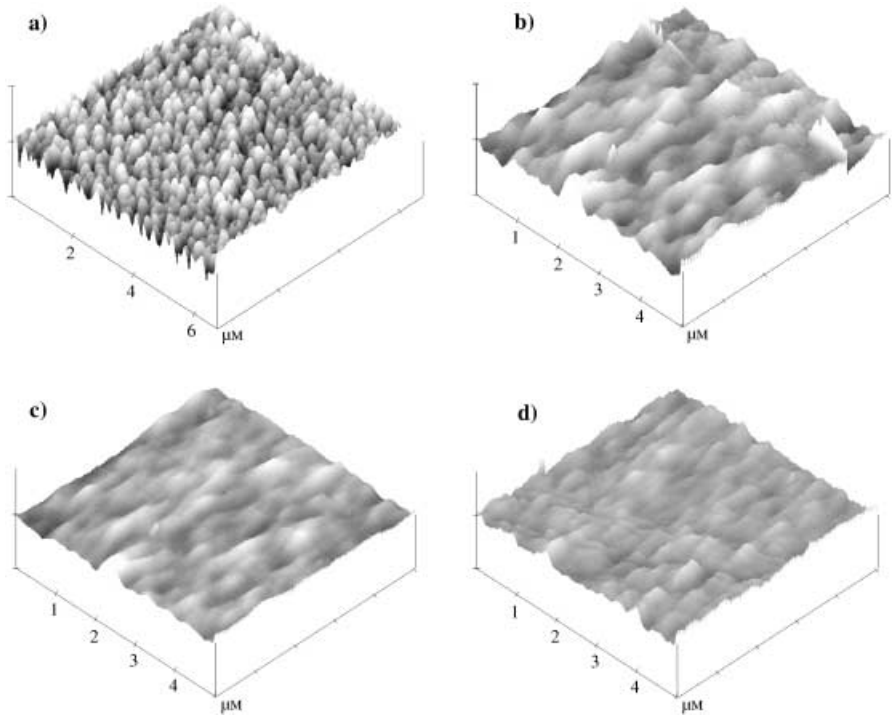

Figure 1. AFM images of 5×5 μm samples: a) bare ITO plate (RMS roughness value of the coating (R_a = 7.622 nm, *z* scale: 80 nm)), b) dip-coated ITO (R_a = 0.615 nm, *z* scale: 20 nm), c) coated ITO on applying −0.9 V for 30 min (R_a = 0.568 nm, *z* scale: 20 nm), and d) coated ITO on applying −1.4 V for 30 min (R_a = 0.522 nm, *z* scale: 20 nm). All coated surfaces were dried for one week at room temperature after the deposition stage.

Factors affecting film deposition

Applied potential: Controlling film thickness is a nontrivial task in practically all methods of coating.[1,2,7,10,11] Figure 2 shows the convenient control of film thickness, ranging from several tens of nanometers (a film thickness of 55 nm is obtained by simple dip coating) up to several hundreds of nanometers, by variation of the applied potential. Film growth is more sensitive to negative than to positive potentials, as will be discussed below. The positive potential is limited (on ITO) to +2.5 V versus Ag/AgBr, because considerable oxygen evolution occurs beyond this voltage, while the negative potential is limited to −1.6 V, beyond which massive hydrogen evolution occurs. The presence of phenolphthalein in solution A resulted in the formation of a pink color near the electrode surface on applying potentials more negative than −1.0 V. The color became darker as the potential was made either more negative or applied for a longer period.

Amount of added water: As can be seen in Figure 3, the effect of added water on thickness passes through a maximum on applying negative or positive potentials for 30 min. The fact that almost no film is deposited when no water is added is very important and is discussed below. Moreover, we draw attention to the similarity in behavior under acidic and alkaline conditions, which suggests that the role played by water is similar in both potential regions.

Duration of the applied potential: The influence of the time for which the potential was applied on the film thickness is shown in Figure 4 for negative

 © 2004 Wiley-VCH Verlag GmbH & Co. KGaA, Weinheim

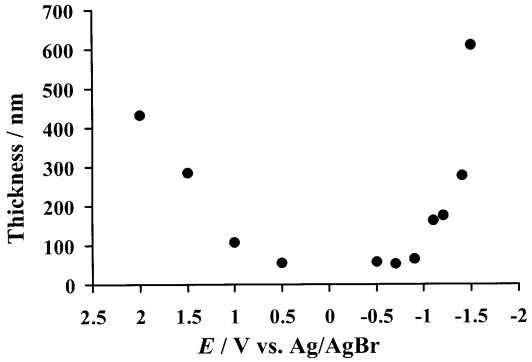

Figure 2. Thickness of zirconia electrodeposited films as a function of the applied potential. All potentials were applied for 30 min with slow stirring of solution A (see Experimental Section). Unless otherwise stated, this solution was used in the other figures as well.

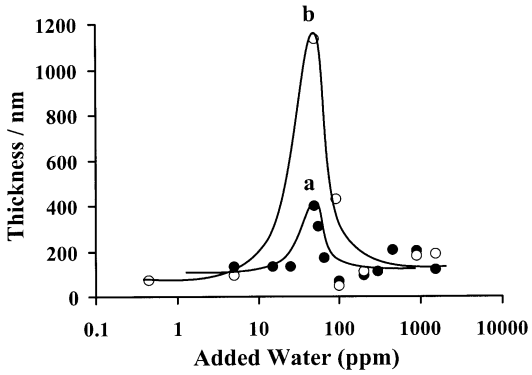

Figure 3. Effect of added water on the thickness of the electrodeposited zirconia films after applying a) −1.2 V and b) +2.5 V for 30 min.

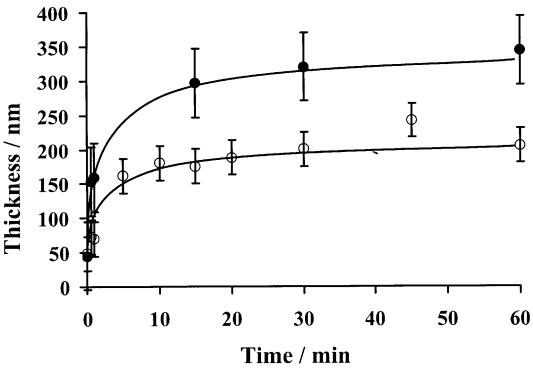

Figure 4. Rate of ZrO_2 film buildup on ITO surfaces on applying −1.2 V (open circles) or +2.5 V (filled circles).

(−1.2 V) and positive potentials (+2.5 V). In both regimes, during the first 15 min or so the films are rapidly built up, after which an almost constant thickness is reached.

Figure 5 shows the effect of negative applied potential on the current–time behavior. Similar behavior was observed for positive potentials. Formation of the film is accompanied by a decrease in the current, which is due to gradual blocking of the electrode surface towards the electroactive species. As the current varies linearly with the concentration gradient of the electroactive species at the electrode surface,

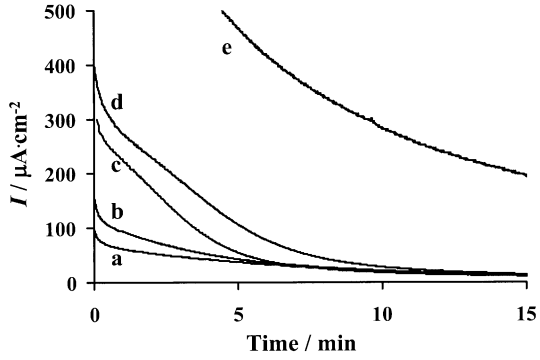

Figure 5. Effect of the applied negative potential on initial current densities and on current decay profiles at ITO electrodes: a) −1.0 V, b) −1.2 V, c) −1.4 V, d) −1.5 V, and e) at a gold electrode (−1.4 V). Note that the currents in lines a–d merge after approximately 15 min.

this clearly suggests that as the film grows, thickens and is cross-linked it becomes less permeable to the species being oxidized or reduced (see below). Due to constant stirring of the solution, such a decrease in the current is not observed in the absence of the zirconium monomer. Water depletion as another plausible explanation of the decay was ruled out, as doubling the water content by injecting an additional 900 ppm of water after 30 min had no apparent effect on the current. Interestingly, although the initial current density increases as the applied potential becomes more negative, the curves eventually merge (after 10–15 min), and similar current densities result. This suggests that the film grows quickly during the first 10–15 min of applying the potential, and that the steady-state current attained after this time has almost no effect on film growth and originates from its porosity. Therefore, the decrease in the current could be a good indicator for film growth (see below).

Interestingly, two independent measurements could be correlated to an approximate straight line, namely, the thickness (Figure 4) and the current density (Figure 5b), as obtained by applying −1.2 V for different durations (Figure 6).

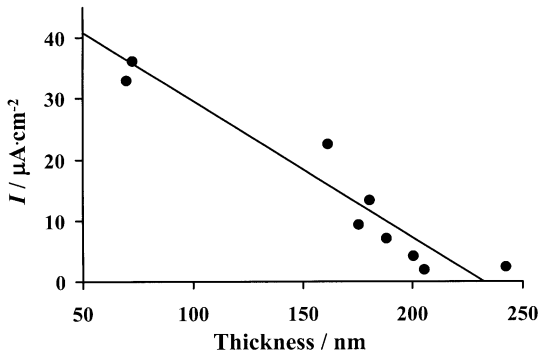

Figure 6. Cathodic current densities versus thickness of the film when −1.2 V versus Ag/AgBr was applied at ITO electrodes. The data were taken from Figures 5b and 4, respectively. The line is only to guide the eye.

Similar results (not shown) were obtained for gold, on which zirconia was deposited by applying −1.4 V. Film growth on gold also ceased after about 15 min, and the cur-

© 2004 Wiley-VCH Verlag GmbH & Co. KGaA, Weinheim

rent density correlated reciprocally with film thickness. These findings again indicate that the decay of current in both systems is due to the gradual blocking of the electrode surfaces during film deposition.

The conducting substrate: Under comparable conditions of preparation films deposited on ITO are significantly thinner than those deposited on gold (Table 1), because the reduction kinetics are more facile on gold than on ITO (Figure 5, curve e). This observation also seems to rule out an electrophoretic mechanism, which would favour the surface with the lower rate of electron transfer, that is, higher overpotential, namely, ITO (see explanation in ref. [24]). The fact that simple dip coating resulted in a similar film thickness for both substrates corroborates the electrochemical origin of film growth.

Table 1. Dependence of film thickness on the method of deposition and the electrode material.

Method	Thickness [nm]	
	on ITO	on gold
dip coating	50±10	60±10
−0.9 V, 30 min	70±10	100±10
−1.4 V, 30 min	280±10	560±10

Furthermore, comparison of the current decays during buildup of the films on ITO and gold electrodes (Figure 5, curves c and e) shows that the decrease in reduction current density for gold is much steeper than that for ITO. This also suggests that electrochemical deposition of the gel is faster on gold than on ITO. In addition, the current densities measured at the steady state (>15 min) are also different: the gold electrode exhibits higher current densities than ITO. Nevertheless, these steady-state currents do not lead to substantial film thickening.

Stirring speed: With decreasing stirring speed, the films thicken. Nonetheless, we maintained a constant stirring speed to avoid inhomogeneities in the deposited films. The fact that the thickness of the deposited films decreased with increasing stirring speed suggests that deposition depends on the formation of a local gradient of electrogenerated species (i.e., OH^- and H^+), which is strongly affected by convection. On the other hand, it indicates that formation of the film is not limited by mass transport to the film/electrolyte interface, which should be enhanced by stirring the solution.

Electrochemical studies

Our findings clearly indicate that the sol–gel films are deposited as a result of applying either positive or negative potentials. Moreover, Faradaic processes, that is, oxidation and reduction of electroactive species, and not charging of the electrode surface, are responsible for drastically enhancing the rate of film deposition. Therefore, we primarily tried to determine the oxidation and reduction processes and the products that account for this electrocatalytic deposition process.

Figure 7 shows the cyclic voltammogram of an ITO electrode in 2-propanol and 0.1 M $LiClO_4$ before and after adding 900 ppm of water and 1.12 M $[Zr(OPr)_4]$. The reduction and oxidation of 2-propanol commence at potentials more negative than −1.0 V and more positive than +2.0 V, respectively. Evidently, the addition of water (Figure 7b) significantly increases the currents associated with the reduction and oxidation waves; however, these diminish as soon as the monomer $[Zr(OPr)_4]$ is added, presumably because of its reaction with water. Note that $[Zr(OPr)_4]$ is not electroactive in this potential window. Therefore, one has to take into account the electroactivity of the solvent and the added water. The reduction of 2-propanol is likely to give the alkoxide ion,[29] and therefore, the two reduction processes are given by Equations (1) and (2).

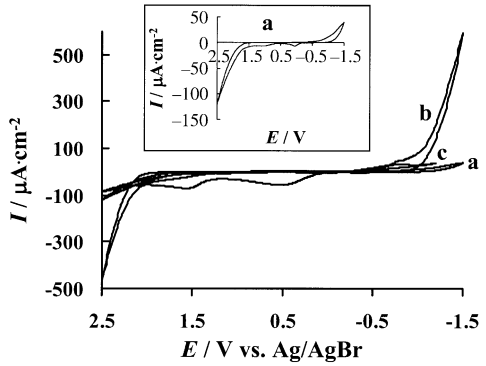

Figure 7. Cyclic voltammetry of an ITO plate in 0.1 M $LiClO_4$ solution of: a) dry *i*PrOH, b) *i*PrOH with 900 ppm (0.05 M) water and c) *i*PrOH with 0.05 M water and 1.12 M $[Zr(OPr)_4]$.

$$Me_2CHOH + e^- \rightarrow Me_2CHO^- + {}^1/_2\,H_2 \quad (1)$$

$$H_2O + e^- \rightarrow {}^1/_2\,H_2 + OH^- \quad (2)$$

The electrochemically generated alkoxide will react with water to yield hydroxyl ions [Eq. (3)].

$$Me_2CHO^- + H_2O \rightarrow Me_2CHOH + OH^- \quad (3)$$

The anodic processes increase the local concentration of protons by generating ketone[29] or oxygen [Eqs. (4) and (5)].

$$Me_2CHOH \rightarrow Me_2CO + 2\,H^+ + 2\,e^- \quad (4)$$

$$H_2O \rightarrow {}^1/_2\,O_2 + 2\,H^+ + 2\,e^- \quad (5)$$

Figure 8 shows that indeed both the cathodic (measured at −1.5 V) and anodic (at +2.0 V) currents vary linearly with the amount of added water. However, while the anodic current vanishes as water is eliminated, the cathodic background current is significant. This suggests that the reduction of the *i*PrOH contributes more to the total current than its oxidation. Moreover, this observation, along with the number of electrons that are involved in the reduction and

 © 2004 Wiley-VCH Verlag GmbH & Co. KGaA, Weinheim

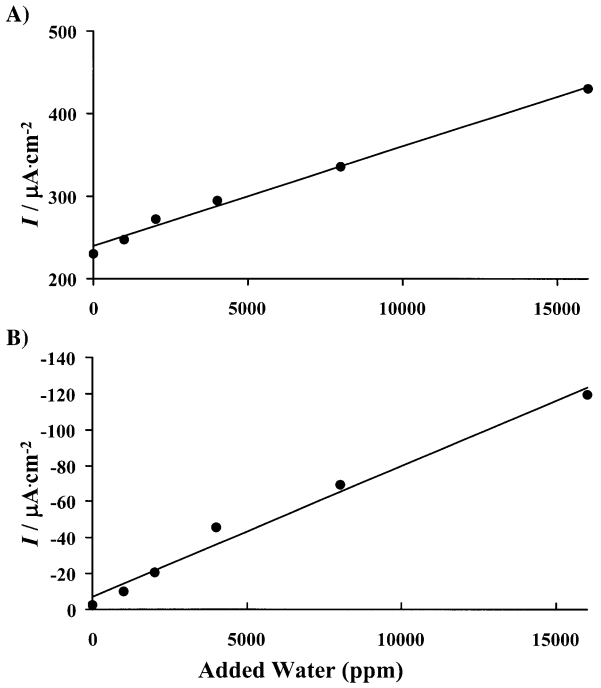

Figure 8. A) Cathodic and B) anodic current densities versus amount of water added to dry *i*PrOH + 0.1 M $LiClO_4$ solution.

oxidation of water [Eqs. (2) and (5), respectively] account for the increase in the cathodic and anodic currents by factors of 2 and 15, respectively, upon adding 0.9 M (16000 ppm) of water.

In view of the high reactivity of $[Zr(OPr)_4]$ towards water and the low concentration ratio ($r = 10^{-5}$–10^{-1}) one might expect that all of the added water would disappear by hydrolyzing the monomer to (mono)hydroxylated zirconium propoxide species with liberation of PrOH [Eq. (6)]. However, since film growth is evident only in the presence of water (see Figure 3) it seems that some of the water remains in the system as such. This can be understood by recalling that the solvent, *n*PrOH and *i*PrOH, is in such large excess over water that the hydrolysis equilibrium is quenched and some of the water is retained as a free reagent [Eq. (6)], in accordance with Le Châtelier's principle.

$$Zr(OPr)_4 + x\,H_2O \rightleftarrows Zr(OPr)_{4-x}(OH)_x + x\,PrOH \qquad (6)$$

This process has an equilibrium constant of $K \approx 1700$,[30] from which it can be deduced that although most of the water in the solution is consumed, a small fraction still remains as free water. Employing high initial concentrations of the monomer and solvent (1.12 M and 8.5 M, respectively) while introducing low concentration of water (0.05 M) results in an equilibrium concentrations of water of about 0.2 mM (only 0.4 % of its initial value) and of the monohydroxylated species of about 0.05 M. Indeed, Figure 7 shows that the cathodic and anodic signals significantly decrease on adding the monomer to the mixture of water and 2-propanol. The only significant process that one might expect is the conversion of $[Zr(OPr)_4]$ to mixed $[Zr(OPr)_x(O\text{-}2\text{-}Pr)_{4-x}]$ alkoxides. Since this mixed alkoxide behaves esentially like the original alkoxide, we shall continue to use the notation $[Zr(OPr)_4]$ below, where OPr refers to *n*Pr or 2-Pr groups. This means that at least the cathodic current (Figure 5) which is measured in the presence of the monomer is mainly due to PrOH reduction. This is in accordance with our findings that added water had no significant effect on the measured current.

To better understand how film growth affects the current, we studied the current decay under well-controlled conditions using a gold disk electrode (Figure 9). We applied

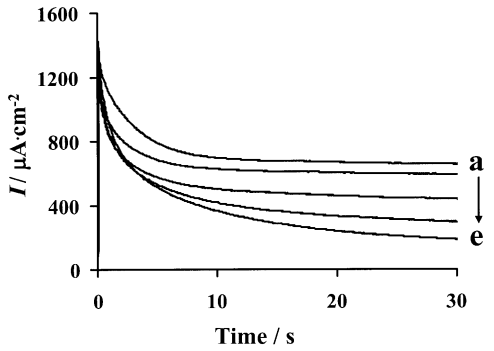

Figure 9. Current–time transients recorded with a gold electrode in solution A. The potential was stepped from 0 V to −1.2 V at different times during film deposition: a) first 3 min to e) after 12 min of deposition.

−1.2 V for 3 min in five successive periods. It is evident that as deposition proceeds, the current decreases. This decrease is diffusion-controlled, as is evident from the linear dependence on $t^{-1/2}$ (not shown). We used a simple model, based on two resistors in series, to represent the film and the solution (Figure 10). Therefore, the respective currents can be treated by the Savéant approach[31] [Eq. (7)], where i_{Total}, $i_{Solution}$ and i_{Film} are the total current, the current that is controlled by the gradient formed in solution and the current controlled by transport in the film, respectively.

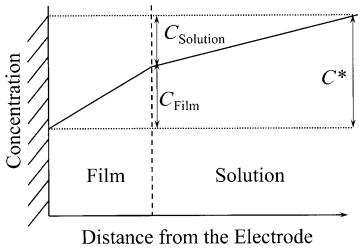

Figure 10. Schematic diagram of the concentration gradient of electroactive species that is formed during film deposition. For symbols, see text.

$$\frac{1}{i_{total}} = \frac{1}{i_{solution}} + \frac{1}{i_{film}} \qquad (7)$$

Assuming diffusion-controlled conditions gives Equation (8),

© 2004 Wiley-VCH Verlag GmbH & Co. KGaA, Weinheim

$$\frac{1}{i_{total}} = \frac{\pi^{1/2} t^{1/2}}{nFAD_{solution}^{1/2} C_{solution}} + \frac{\delta}{nFAD_{film} C_{film}} \quad (8)$$

where n is the number of electrons that are exchanged per molecule [$n=1$, see Eq. (1)], F the Faraday constant, A the electrode area (0.07 cm^2), t the measurement time, $D_{solution}$, D_{film} and $C_{solution}$, C_{film} are the diffusion coefficients and the concentration gradients of the species in solution and in the film, respectively, and δ is the film thickness. Clearly, the sum of $C_{solution}$ and C_{film} (Figure 10) is equal to the total concentration gradient of the species between the electrode and the bulk [Eq. (9)].

$$C_{solution} + C_{film} = C^* \quad (9)$$

Therefore, plotting i^{-1} as a function of $t^{1/2}$ [Eq. (8)] should result in a linear dependence, whereby the slope and the intercept are given by Equations (10) and (11).

$$\text{slope} = \frac{\pi^{1/2}}{nFAD_{solution}^{1/2} C_{solution}} \quad (10)$$

$$\text{Intercept} = \frac{\delta}{nFAD_{film} C_{film}} \quad (11)$$

Indeed, all curves recorded after a known time of applying a negative potential gave a linear plot of i^{-1} as a function of $t^{1/2}$ (Figure 11), but with different slopes and intercepts.

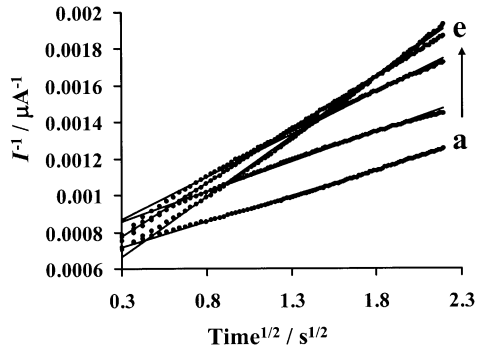

Figure 11. Dependence of the reciprocal current from Figure 9 on $t^{1/2}$.

Extracting the slope and introducing the diffusion coefficient of propanol ($D_{solution} = 1.6 \times 10^{-5}$ $cm^2 s^{-1}$[32] allows $C_{solution}$, *and therefore* C_{film}, to be calculated for each curve. Introducing the latter value to the intercept of each curve [Eq. (11)] made it possible to determine D_{film}, given δ from profilometry. As expected, we obtained a constant diffusion coefficient, $D_{film} = (2.2 \pm 0.7) \times 10^{-8}$ $cm^2 s^{-1}$, for the solvent in the film.

Finally, the permeability of the films towards conventional one-electron redox couples was examined. Three species were used: hexacyanoferrate(II), hexaammineruthenium(II), and ferrocene, of which the first two are hydrophilic and the last-named is hydrophobic. The redox responses of $[Fe(CN)_6]^{3-}$ and $[Fe(C_5H_5)_2]$ at freshly deposited films (treatment a as detailed in the Experimental Section) are shown in Figure 12. These voltammograms show that the electrochemistry of $[Fe(C_5H_5)_2]$ is practically unaffected by the wet zirconia film, but the hydrophilic species (shown for

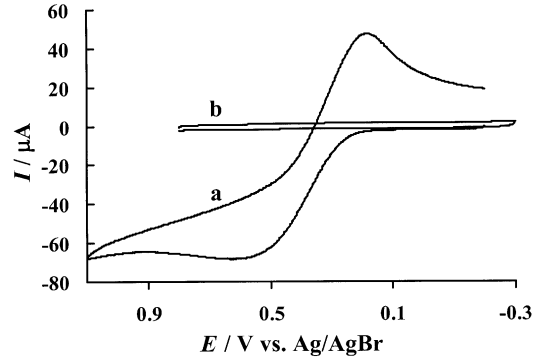

Figure 12. Cyclic voltammetry of a) 5 mM $[Fe(C_5H_5)_2]$ and b) 5 mM $[Fe(CN)_6]^{3-}$ in 0.1 M $LiClO_4$ *i*PrOH solution, recorded with scan rate of 100 mV $s^{-1}$and ITO electrodes (treatment a, as described in the Experimental Section).

$[Fe(CN)_6]^{3-}$) show no penetration at all (the currents of $[Fe(C_5H_5)_2]$ and $[Fe(CN)_6]^{3-}$ on bare ITO are 140 and 125 μA, respectively). As for treatments c and d, the hydrophilic species exhibited higher currents, while the currents that originated from the electrochemistry of $[Fe(C_5H_5)_2]$ were unchanged. Furthermore, we studied the effect of film deposition on the diffusion coefficient of $[Fe(C_5H_5)_2]$. The results were unquestionable: the diffusion coefficient of ferrocene was not affected by the growth of the film, as verified by chronoamperometry ($D \approx 3.7 \times 10^{-5}$ $cm^2 s^{-1}$).[33] All of these findings imply that the freshly formed zirconia film exhibits a certain degree of hydrophobicity, which might be due to the first, strongly adsorbed layer of propanol, and perhaps also to some incomplete hydrolysis of the monomer leaving ZrOPr residues. Indeed, the hydrophobicity decreases as a result of exposure to the atmosphere. The separation between the oxidation and reduction waves of $[Fe(C_5H_5)_2]$ (ca. 400 mV) in Figure 11 is mainly due to sluggish kinetics at the ITO/solution interface. Replacing ITO by gold, which exhibits faster kinetics, decreases the potential peak separation.

Proposed polycondensation mechanism

In view of the above results, we propose adopting the mechanism that is commonly accepted for ZrO_2 sol–gel formation with catalysis under acidic or alkaline conditions.[34–36] Clearly, the electrochemical processes eventually generate H^+ or OH^- [Eqs. (1)–(5)]. Although protons and hydroxide ions are generated electrochemically even in the absence of water, water is crucial for the deposition of a zirconia film (Figure 3). This implies that water is involved not only in the electrochemical reaction but also in the condensation itself [Eqs. (12) and (13)]. Specifically, under oxidative conditions, H^+ is formed, which then protonates $[Zr(OPr)_4]$ to $[Zr(OPr)_3(PrOH)]^+$. Nucleophilic substitution takes place with water to give $[Zr(OPr)_3(H_2O)]^+$ [Eq. (12)]. The monoprotonated species condenses to form Zr-O-Zr bonds by

 © 2004 Wiley-VCH Verlag GmbH & Co. KGaA, Weinheim

reacting with another monomer molecule (either hydrolyzed or not), releasing either a water molecule, propyl alcohol or dipropyl ether [e.g., Eq. (13)].

$$[Zr(OPr)_3(PrOH)]^+ + H_2O \rightarrow [Zr(OPr)_3(OH_2)]^+ + PrOH \quad (12)$$

$$[Zr(OPr)_3(OH_2)]^+ + [Zr(OPr)_4] \rightarrow [Zr(OPr)_3OZr(OPr)_3]+ PrOH + H^+ \quad (13)$$

Under reductive conditions, it is OH^- which forms $[Zr(OPr)_3(OH)]$ by nucleophilic substitution, releasing PrO^- [Eq. (14)]; the monohydroxylated species condenses with another monomer to form Zr-O-Zr bonds by a hydrolytic mechanism [Eq. (15)][34,36]). Hence, the role played by water is primarily to provide the nucleophile, which attacks zirconium and forms $[Zr(OPr)_3(OH)]$. The fact that most of the cathodic current is attributed to the reduction of the solvent supports this claim.

$$[Zr(OPr)_4] + OH^- \rightarrow [Zr(OPr)_3OH] + PrO^- \quad (14)$$

$$[Zr(OPr)_3OH] + [Zr(OPr)_4] \rightarrow [Zr(OPr)_3OZr(OPr)_3] + PrOH \quad (15)$$

The fact that the film ceased growing after reaching a certain thickness, which depends primarily on the nature of the electrode material, is apparently due to the flux profile of the electrogenerated species. Clearly, the lower the overpotentials for solvent oxidation and reduction, the larger the fluxes of these species are. In other words, as the flux of protons or hydroxyl ions increases, the reaction zone will extend farther into the solution. Yet, as the film is built, it slows down significantly the diffusion of both the solvent and water and hence decreases the rate of film deposition. The film will presumably grow until it reaches the diffusion layer of the electrogenerated protons or hydroxyl ions. Increasing the flux by applying more negative or positive potentials pushes this layer deeper into the solution. On the other hand, it is evident that a certain concentration of H^+ or OH^- is required at the film/electrolyte interface to drive film growth. Convection of the solution tends to level this pH gradient and therefore decreases the rate of film deposition.

An issue which is still unresolved is the complex effect of water concentration on film thickness (Figure 3). It is evident from Figure 2 that the rate of H^+ or OH^- generation governs the rate of film deposition, but this depends on the potential and only to a lesser extent on water concentration. In other words, the concentration of water must be above a certain level so that, on one hand, every RO^- that is electrochemically formed will immediately react with water to form OH^-, and on the other hand, that the species $Zr(OPr)_4$ will be able to undergo nucleophilic attack by water to form $[Zr(OPr)_3(H_2O)]^+$. An initial current density of about 100 $\mu A\,cm^{-2}$ (approximately equal to a flux of $10^{-9}\,mol\,s^{-1}\,cm^{-2}$) and a diffusion path of 10 μm would result in a concentration of 1 mM of generated electroactive species. Therefore, the relatively small amounts of water (in the 0.1 mM range) will be fully consumed. Yet, we do not have a clear explanation for the fact that higher concentrations of water tend to decrease the film thickness.

Conclusion

Our study clearly shows that electrochemical reactions that take place at the interface of conducting substrates result in the formation of zirconium oxide thin films with thickness in the submicrometer range. The effect of the different parameters that control the growth of the film on ITO and Au surfaces suggests a mechanism of electrochemical acid or base catalysis. The major advantage of this approach is the ability to control the deposition rate externally by means of the applied potential. However, the formation of thick films, in the micrometer range, is limited due to hindrance of diffusion of the electroactive species to the electrode surface and of the protons and hydroxyl ions from the electrode to the solution by the deposited film. In other words, the process is self-controlled and ceases as the pH at the film/electrolyte interface becomes insufficient to drive film deposition. This also implies that the reported approach could be advantageous for depositing films on the nanometer scale on conducting surfaces.

Experimental Section

Chemicals: Zirconium tetra-*n*-propoxide ($[Zr(OPr)_4]$, 70% (w/w) in *n*-propanol, ABCR) was used as received. Highly pure $LiClO_4$, KNO_3, KBF_4, and NaCl were purchased from Merck. 2-propanol (2-PrOH) was dried over 0.3 nm molecular sieves for at least one week, which resulted in a water content of less than 1 ppm (determined by the Karl Fischer method). Highly purified water (EasyPure U.V., Barnstead) with resistivity of 18.3 MΩcm was used in all experiments. Phenolphthalein, $K_3[Fe(CN)_6]$, $[Ru(NH_3)_6]Cl_3$ and ferrocene were obtained from Aldrich. The conducting substrates were indium tin oxide on glass (ITO, Delta Technologies Stillwater, MN) or thin gold films (ca. 2000 Å) deposited on glass that was previously covered with a thin (ca. 5 nm) chromium layer. The areas of ITO electrodes were ca. 1.2 cm^2 in Figures 1–8, 11, and 12. The area of all gold substrates was 0.07 cm^2.

Electrochemical experiments were performed with a VersaStat potentiostat (EG&G). Cyclic voltammetry (CV) and chronoamperometry (CA) were performed in a conventional three-electrode cell with a graphite rod as auxiliary electrode and an Ag/AgBr wire as the reference electrode. All potentials quoted here are versus this reference electrode, that is about +70 mV versus standard hydrogen electrode (SHE). The deposition solution consisted of 1.12 M $[Zr(OPr)_4]$ to which 0.1 M $LiClO_4$ in 2-propanol and 900 ppm of water ($r = 0.045$) were added (solution A). Constant potentials were applied to the substrates in the range of +2.5 V to −1.5 V with continuous, slow stirring for 0.5–90 min. The substrates were withdrawn from the deposition solution by a homemade lifter at a rate of 50 $\mu m\,s^{-1}$ while constantly applying the potential. The films were dried at room temperature for at least 24 h.

For electrochemical characterization of the deposited films we used dry 2-propanol solutions that contained 0.1 M $LiClO_4$ and 5 mM of the electroactive species: hexacyanoferrate(II), hexaammineruthenium(II) or ferrocene. Voltammograms of each species were recorded a) Immediately after deposition, b) After immersing the fresh gels in 2-PrOH for 3 h, c) After immersing the fresh gels in the solution of the electroactive spe-

© 2004 Wiley-VCH Verlag GmbH & Co. KGaA, Weinheim

cies for 3 h, and d) After drying the films for a week at room temperature.

Other instrumentation: The thickness of the deposited films was measured with a profilometer (P-15, KLA-Tencor Co.). AFM images were acquired with a NanoScopeII (Digital Instruments, CA), operated in the contact mode using a cantilever with a spring constant of $0.58\,N\,m^{-1}$. Scanning electron micrographs and elemental analyses were acquired with a JEOL JSM-6400 SEM with an electron-beam intensity of 15 or 10 keV. XRD spectra were recorded with a PW1710 diffractometer at 40 kV and 35 mA in the range of $20 < 2\theta < 63°$.

Acknowledgement

This project was supported by the Israel Ministry for Science, Sports and Arts, through the Tashtiot Projects (projects 2042 and 1095), and by a Robert Szold Fund. Prof. L. Ben-Dor is gratefully acknowledged for the XRD measurements.

[1] a) A. T. Kuhn, C. Y. Chan, *J. Appl. Electrochem.* **1983**, *13*, 189–207; b) G. H. A. Therese, P. V. Kamath, *Chem. Mater.* **2000**, *12*, 1195–1204.
[2] G. R. Lee, J. A. Cryston, *J. Mater. Chem.* **1996**, *6*, 187–192.
[3] a) J. A. Switzer, *Am. Ceram. Soc. Bull.* **1987**, *66*, 1521–1524; b) D. Aslanidis, J. Frasaer, J.-P. Celis, *J. Electrochem. Soc.* **1997**, *144*, 2352–2357; c) J. A. Switzer, M. J. Shane, R. J. Phillips, *Science* **1990**, *247*, 444–446.
[4] S. K. Yen, *J. Electrochem. Soc.* **1999**, *146*, 1392–1396.
[5] I. Serebrennikova, V. I. Birss, *J. Electrochem. Soc.* **1997**, *144*, 566–572.
[6] P. Slezak, A. Wieckowski, *J. Electrochem. Soc.* **1991**, *138*, 1038–1040.
[7] G. H. A. Therese, P. V. Kamath, *Chem. Mater.* **1998**, *10*, 3364–3367.
[8] a) S. K. Yen, *Mater. Chem. Phys.* **2000**, *63*, 256–262; b) J. A. Switzer, M. G. Shumsky, E. W. Bohannan, *Science* **1999**, *284*, 293–296; c) Z. H. Gu, T. Z. Fahidy, *J. Electrochem. Soc.* **1999**, *146*, 156–159.
[9] J. Gobet, H. Tannenberger, *J. Electrochem. Soc.* **1988**, *135*, 109–112.
[10] G. H. A. Therese, P. V. Kamath, *Chem. Mater.* **1999**, *11*, 3561–3564.
[11] Y. Matsumoto, Y. Ishikawa, M. Nishida, S. Ii, *J. Phys. Chem. B* **2000**, *104*, 4204–4209.
[12] a) T. Yoshida, H. Minoura, *Adv. Mater.* **2000**, *12*, 1219–1222; X. Y. Zhang, L. D. Zhang, W. Chen, G. W. Meng, M. J. Zheng, L. X. Zhao, F. Phillipp, *Chem. Mater.* **2001**, *13*, 2511–2515.
[13] J. H. Fendler, *Nanoparticles and Nanostructured Films*, Wiley-VCH, **1998**, Chap. 3, 53–69.
[14] a) I. Zhitomirsky, L. Gal-Or, *Electrochemical Coatings in Intermetallic and Ceramic Coatings*, Marcel-Dekker, New York, **1999**; b) K. Bandyopadhyay, K. Vijayamohanan, *Langmuir* **1998**, *14*, 6924–6929; c) M. Aslam, S. Pethkar, K. Bandyopadhyay, I. S. Mulla, S. R. Sainkar, A. B. Mandale, K. Vijayamohanan, *J. Mater. Chem.* **2000**, *10*, 1737–1743; d) H.-Z. Yu, A. W. Rowe, D. M. Waugh, *Anal. Chem.* **2002**, *74*, 5742–5747.
[15] R. Chaim, I. Silberman, L. Gal-Or, *J. Electrochem. Soc.* **1991**, *138*, 1942–1946.
[16] L. Gal-Or, I. Silberman, R. Chaim, *J. Electrochem. Soc.* **1991**, *138*, 1939–1942.
[17] a) H. Nishimori, M. Tatsumisago, T. Minami, *J. Ceram. Soc. Jpn.* **1995**, *103*, 78–80; b) H. Nishimori, K. Hasegawa, M. Tatsumisago, T. Minami, *J. Sol-Gel Sci. Techn.* **1996**, *7*, 211–216.
[18] H. Nishimori, M. Tatsumisago, T. Minami, *J. Mater. Sci.* **1996**, *31*, 6529–6533.
[19] a) K. Hasegawa, M. Tatsumisago, T. Minami, *J. Ceram. Soc. Jpn.* **1997**, *105*, 569–572; b) K. Hasegawa, S. Kunugi, M. Tatsumisago, T. Minami, *Chem. Lett.* **1997**, 1115–1116.
[20] K. Hasegawa, H. Nishimori, M. Tatsumisago, T. Minami, *J. Mater. Sci.* **1998**, *33*, 1095–1098.
[21] K. Katagiri, K. Hasegawa, A. Matsuda, M. Tatsumisago, T. Minami, *J. Am. Ceram. Soc.* **1998**, *81*, 2501–2503.
[22] a) D. E. Clark, W. J. Dalzell, D. C. Folz, *Ceram. Eng. Sci. Proc.* **1988**, *9*, 1111–1118; b) J. Laubersheimer, H.-J. Ritzhaupt-Kleissl, J. Hauselt, G. Emig, *J. Europ. Ceram. Soc.* **1998**, *18*, 255–260.
[23] K. Hasegawa, S. Kunugi, M. Tatsumisago, T. Minami, *J. Sol-Gel Sci. Techn.* **1999**, *15*, 243–249.
[24] K. M. Liang, W. L. Huang, S. R. Gu, *Mater. Res. Bull.* **2000**, *35*, 115–123.
[25] R. Shacham, D. Avnir, D. Mandler, *Adv. Mater.* **1999**, *11*, 384–388.
[26] M. Guglielmi, A. Licciulli, S. Mazarelli, *Cer. Acta* **1994**, *6*, 19.
[27] a) M. Agarwal, M. R. De Guire, A. H. Heuer, *J. Am. Ceram. Soc.* **1997**, *80*, 2967–2981; b) A. D. Polli, T. Wagner, A. Fischer, G. Weinberg, F. C. Jentoft, R. Schlögl, M. Rühle, *Thin Solid Films* **2000**, *379*, 122–127.
[28] a) P. C. Innocenzi, M. Guglielmi, M. Gobbin, P. Colombo, *J. Eur. Ceram. Soc.* **1992**, *10*, 431–436; b) P. Audebert, S. Bertrand, F. Bresson, G. Tribillon, *Appl. Surf. Sci.* **1997**, *119*, 207–214; c) E. Giorgetti, G. Margheri, S. Sottini, M. Casalboni, R. Senesi, M. Scarselli, R. Pizzoferrato, *J. Non-Cryst. Solids* **1999**, *255*, 193–198; d) C. Veytizou, J.-F. Quinson, A. Douy, *J. Mater. Chem.* **2000**, *10*, 365–370; e) Z. Xuping, L. Qing, Z. Haokang, *J. Electron. Mater.* **1998**, *27*, 1347–1350.
[29] M. M. Baizer, H. Lund, *Organic Electrochemistry: An Introduction and a Guide*, 2nd ed., Marcel Dekker, New York, **1983**.
[30] D. E. Richardson, G. H. L. Lang, E. Crestoni, M. F. Ryan, J. R. Eyler, *Int. J. Mass Spectrom.* **2001**, *204*, 255–266.
[31] C. P. Andrieux, J. -M. Savéant, *Molecular Design of Electrode Surfaces, Vol. 22*, Wiley, New York, **1992**.
[32] K. R. Harris, P. J. Newitt, *J. Phys. Chem. B* **1998**, *102*, 8874–8879.
[33] P. Audebert, S. Sallard, S. Sadki, *J. Phys. Chem. B* **2003**, *107*, 1321–1325.
[34] a) C. J. Brinker, G. W. Scherer, *Sol Gel Science*, Academic Press, San Diego, CA, **1990**; b) D. Avnir, *Acc. Chem. Res.* **1995**, *28*, 328–334; c) A. M. Buckley, M. Greenblatt, *J. Chem. Educ.* **1994**, *71*, 599–602; d) L. L. Hench, J. K. West, *Chem. Rev.* **1990**, *90*, 33–72; e) J. Livage, C. Sanchez, *J. Non-Cryst. Solids* **1992**, *145*, 11–19.
[35] a) M. Ritala, K. Kukli, A. Rahtu, P. I. Raisanen, M. Leskela, T. Sajavaara, J. Keinonen, *Science* **2000**, *288*, 319–321; b) M. Z.-C. Hu, J. T. Zielke, C. H. Byers, J. S. Lin, M. T. Harris, *J. Mater. Sci.* **2000**, *35*, 1957–1971; c) M. C. Caracoche, P. C. Rivas, M. M. Cervera, R. Caruso, E. Benavidez, O. De Sanctis, M. E. Escobar, *J. Am. Ceram. Soc.* **2000**, *83*, 377–384; d) R. J. P. Corriu, D. Leclercq, H. P. Mutin, L. Sarlin, A. Vioux, *J. Mater. Chem.* **1998**, *8*, 1827–1833; e) H. Cattey, P. Audebert, C. Sanchez, P. Hapiot, *J. Mater. Chem.* **1997**, *7*, 1461–1466; f) M. J. Percy, J. R. Bartlett, J. L. Woolfrey, L. Spiccia, B. O. West, *J. Mater. Chem.* **1999**, *9*, 499–505; g) K. S. Alber, J. A. Cox, *Mikrochim. Acta* **1997**, *127*, 131–147; h) M. A. Fardad, *J. Mater. Sci.* **2000**, *35*, 1835–1841; i) J. Zhao, W. Fan, D. Wu, Y. Sun, *J. Mater. Res.* **2000**, *15*, 402–406.
[36] a) A. C. Geiculescu, H. G. Spencer, *J. Sol-Gel Sci. Tech.* **1999**, *16*, 243–256; b) H. Hayashi, H. Suzuki, S. Kaneko, *J. Sol-Gel Sci. Tech.* **1998**, *12*, 87–94; c) R. Srinivasan, B. H. Davis, *Materials Synthesis and Characterization*, Plenum Press, New York, **1997**; d) M. J. Percy, J. R. Bartlett, L. Spiccia, B. O. West, J. L. Woolfrey, *J. Sol-Gel Sci. Tech.* **2000**, *19*, 315–319; e) M. J. Percy, J. R. Bartlett, J. L. Woolfrey, L. Spiccia, B. O. West, *J. Mater. Chem.* **1999**, *9*, 499–505.

Received: August 20, 2003
Revised: December 1, 2003 [F5469]

 © 2004 Wiley-VCH Verlag GmbH & Co. KGaA, Weinheim